Supplement of Atmos. Chem. Phys., 23, 203–220, 2023
https://doi.org/10.5194/acp-23-203-2023-supplement

*Supplement of*

# Isothermal evaporation of $\alpha$-pinene secondary organic aerosol particles formed under low $NO_x$ and high $NO_x$ conditions

**Zijun Li et al.**

*Correspondence to:* Annele Virtanen (annele.virtanen@uef.fi)

**Supplement material**

## S1.1 Forward modelling for high-RH cases

To model the particle evaporation at high RH, we applied a liquid-like evaporation model (LLEVAP) (Vesala et al., 1997; Lehtinen and Kulmala, 2003; Yli-Juuti et al., 2017). This model assumes there is no concentration gradient existing in the particle. It solves a series of differential equations which describe mass fluxes of organic compounds between particle and gas phase on the basis of gas-phase diffusion, i.e., the difference in the gas-phase concentration of an organic compound near the particle surface and far away for the particle. In this case, the particle-phase volatility distribution (VD) is the only driving factor for the evaporation rate in the model simulation.

Following Tikkanen et al. (2020), we first derived the VD from the positive matrix factorization (PMF) analysis of the FIGAERO measurements (hereafter $VD_{PMF}$). Afterwards, the derived $VD_{PMF}$ was used as the initial particle-phase VD in the LLEVAP model. The $VD_{PMF}$ was derived from the median desorption temperature values ($T_{50}$), with the interquartile range of desorption temperature ($T_{25} – T_{75}$) in the factor thermograms as the uncertainty. The start time for each LLEVAP simulation was set to the middle time point (i.e., 15 min) of the FIGAERO measurements. In our LLEVAP simulations, we applied the same set of particle properties as Tikkanen et al. (2020). This includes the gas-phase diffusion coefficient, molar mass, particle density, particle surface tension, and mass accommodation coefficient. For each of the two $NO_x$ cases, the LLEVAP simulation is shown in Figure S2a and b. In addition, we included the observation and LLEVPA simulations for α-pinene SOA particle (O : C = 0.69) from Tikkanen et al. (2020), shown in Figure S2c (see also Figure 5a in Tikkanen et al. (2020)). Additionally, Tikkanen et al. (2020) found the best reconstruction of the measured particle evaporation by allowing each PMF factor to vary in the range of $T_{25} – T_{75}$ ($VD_{PMF}$, optimized, green solid line in Figure S2c).

## S1.2 $T_{max}$ – C* calibration

We calibrated the relationship between the desorption temperature with the maximum signal ($T_{max}$) and saturation vapor concentration ($C^*$) by measuring a homologous series of polyethylene glycols (PEGs, PEG 4 – 8) with well characterized saturation vapor pressure ($p_{sat}$) (Krieger et al., 2018; Ylisirniö et al., 2021). For the FIGAERO-CIMS setup used in this study, the $p_{sat}$ value of an observed molecule can be calculated from the $T_{max}$ value with the maximum signal as follows:

$$\ln(p_{sat}) = -0.21 \times T_{max} - 0.62 \tag{S1}$$

## S1.3 Selection of the optimal PMF solution

As non-nitrated organic compounds (labelled as "CHO compounds") dominated in all α-pinene SOA particle samples (Figure S4 and Figure S5), we performed independent PMF analysis on the data set of CHO compounds and the one of organic nitrates (ON). Such approach enables us to not only better resolve ON into factors but also explore the compositional similarities between the low-$NO_x$ and high-$NO_x$ conditions in terms of the CHO compounds. We investigated PMF solutions with up to 15 factors for the data set of CHO compounds and up to 10 factors for the data set of ON, with fpeak values of -0.5, 0, and 0.5. After a thorough inspection of all PMF solutions, the 12-factor solution at fpeak = 0 was chosen for the data set of CHO compounds. For the data set of ON, the eight-factor solution at fpeak = -0.5 was selected. These two selected PMF solutions yielded the most interpretable results. The PMF results and corresponding factor mass spectra for CHO compounds are shown in Figure S6 and Figure S7, and those for ON are presented in Figure S8 and Figure S9.

The quality of PMF solutions was indicated with the goodness-of-fit parameter ($Q/Q_{exp}$) as a function of number of factors in Figure S10. The unscaled residuals, relative residuals, and scaled residuals of the 10 – 12 factor solutions for the CHO compounds are depicted in Figure S11, and those of the five – eight factor solutions for the ON are shown in Figure S12. With a 10-factor PMF solution for the CHO data set or a five-factor solution for ON data set, we already observed relative residuals of less than 5 % for the majority of data and very subtle changes in the $Q/Q_{exp}$. However, increasing from 10 to 12 factors for the CHO compounds improved the reconstruction of peak shapes for many ions and also identified one more meaningful sample factor improving the interpretability of the aqueous phase processes. In the same way, increasing from five to eight factors for the ON resulted in a better reconstruction of peak shapes for many ions and also finding two more meaningful sample factors which captured different types of ON in the samples. Further increasing the number of factors for CHO compounds and ON resulted in either over-splitting an existing sample factor into two or introducing more background factors. Thus, 12 factors were chosen for the data set of CHO compounds, and eight factors for the one of ON.

## S1.4 Estimation of the total mass concentration in gas and particle phase

According to the partitioning theory (Pankow, 1994) for a system in equilibrium between gas and particle phase, the $C^*$ of a sample factor $k$ can be expressed as

$$C_k^* = OA \cdot \frac{G_k}{P_k}, \tag{S2}$$

where OA is the organic particle mass concentration, which was determined from SMPS data, by assuming a particle density of 1.5 µg $m^{-3}$. $G_k$ and $P_k$ represent the mass concentrations of a sample factor $k$ in gas and particle phase, respectively.

Rearranging Eq. (1), we can calculate the total mass concentration of a sample factor $k$ in both gas and particle phase as follows

$$G_k + P_k = (OA + C_k^*) \cdot \frac{P_k}{OA} \tag{S3}$$

The $C^*$ value of a sample factor $k$ can be estimated by converting its $T_{50}$ value into $C^*$ at 25 °C with a parametrization derived from the $T_{max}$ – $C^*$ calibration. $\frac{P_k}{OA}$ is the mass contribution of a sample factor $k$ in the initial particles prior to isothermal evaporation. Here, we use the mass fraction of a sample factor $k$ in the low-RH, fresh samples as the proxy of $\frac{P_k}{OA}$, since these particle samples experienced the minimum amount of isothermal evaporation.

## SI References

Krieger, U. K., Siegrist, F., Marcolli, C., Emanuelsson, E. U., Gobel, F. M., Bilde, M., Marsh, A., Reid, J. P., Huisman, A. J., Riipinen, I., Hyttinen, N., Myllys, N., Kurten, T., Bannan, T., Percival, C. J., and Topping, D.: A reference data set for validating vapor pressure measurement techniques: Homologous series of polyethylene glycols, Atmos. Meas. Tech., 11, 49-63, 10.5194/amt-11-49-2018, 2018.

Lehtinen, K. E. J. and Kulmala, M.: A model for particle formation and growth in the atmosphere with molecular resolution in size, Atmos. Chem. Phys., 3, 251-257, DOI 10.5194/acp-3-251-2003, 2003.

Pankow, J. F.: An absorption-model of gas-particle partitioning of organic-compounds in the atmosphere, Atmos. Environ., 28, 185-188, Doi 10.1016/1352-2310(94)90093-0, 1994.

Peng, Z. and Jimenez, J. L.: Kinsim: A research-grade, user-friendly, visual kinetics simulator for chemical-kinetics and environmental-chemistry teaching, J. Chem. Educ., 96, 806-811, 10.1021/acs.jchemed.9b00033, 2019.

Tikkanen, O.-P., Buchholz, A., Ylisirniö, A., Schobesberger, S., Virtanen, A., and Yli-Juuti, T.: Comparing secondary organic aerosol (SOA) volatility distributions derived from isothermal SOA particle evaporation data and FIGAERO–CIMS measurements, Atmos. Chem. Phys., 20, 10441-10458, 2020.

Vesala, T., Kulmala, M., Rudolf, R., Vrtala, A., and Wagner, P. E.: Models for condensational growth and evaporation of binary aerosol particles, J. Aerosol Sci, 28, 565-598, Doi 10.1016/S0021-8502(96)00461-2, 1997.

Yli-Juuti, T., Pajunoja, A., Tikkanen, O. P., Buchholz, A., Faiola, C., Vaisanen, O., Hao, L., Kari, E., Perakyla, O., Garmash, O., Shiraiwa, M., Ehn, M., Lehtinen, K., and Virtanen, A.: Factors controlling the evaporation of secondary organic aerosol from alpha-pinene ozonolysis, Geophys. Res. Lett., 44, 2562-2570, 10.1002/2016GL072364, 2017.

Ylisirniö, A., Barreira, L. M. F., Pullinen, I., Buchholz, A., Jayne, J., Krechmer, J. E., Worsnop, D. R., Virtanen, A., and Schobesberger, S.: On the calibration of FIGAERO-ToF-CIMS: Importance and impact of calibrant delivery for the particle-phase calibration, Atmos. Meas. Tech., 14, 355-367, 10.5194/amt-14-355-2021, 2021.

**Table S1**. Summary of experimental conditions and results of α-pinene SOA generation

| | Low-$NO_x$ | High-$NO_x$ |
|---|---|---|
| $[VOC]_{OFR}$ (ppb)[a] | 254 ± 11 | 296 ± 14 |
| $[N_2O]_{OFR}$ (%) | N/A | 1.82 ± 0.10 |
| $[O_3]_{OFR}$ (ppm)[b] | 9.76 ± 0.31 | 6.85 ± 0.36 |
| photon flux ($10^{15}$ photons $cm^{-2}$ $s^{-1}$)[b] | 1.08 ± 0.14 | 2.74 ± 0.35 |
| $T_{OFR}$ (°C) | 24.66 ± 0.76 | 28.14 ± 0.91 |
| $RH_{OFR}$ (%) | 44.19 ± 2.17 | 38.74 ± 2.63 |
| nominal residence time (s) | 160 | 160 |
| effective OH exposure ($10^{12}$ molec $cm^{-3}$ s)[c] | 1.82 ± 0.21 | 2.45 ± 0.09 |
| $\frac{[RO_2]+[NO]}{[RO_2]\ +\ [HO_2]}$ | N/A | 0.84 ± 0.19 |
| fraction Loss to OH (%) | 96 | 50 |
| fraction Loss to $O_3$ (%) | 4 | 1 |
| fraction Loss to $NO_3$ (%) | 0 | 49 |
| oxygen-to-carbon (O:C)[d] | 0.77 ± 0.03 | 0.74 ± 0.01 |
| oxidation state ($OS_c$)[d] | 0.05 ± 0.04 | 0.02 ± 0.02 |

[a] Mixing ratio of α-pinene was corrected with the dilution of $O_3$-contained flow but without the loss due to pure ozonolysis at the inlet. [b] $O_3$ was measured at the OFR outlet after 254-nm UV lamps were switched on but without the addition of α-pinene and $N_2O$. The photon flux was estimated by varying the model input photon flux in the KimSim model (Peng and Jimenez, 2019) until the model output $O_3$ concentration agreed with the measured one. [c] OH exposure was calculated with the KinSim model (Peng and Jimenez, 2019). [d] The values of the oxygen to carbon ratio (O:C) and the oxidation state ($OS_c$) were derived from the HR-ToF-AMS measurement data of monodisperse SOA particles which represents the initial particle population used for isothermal evaporation measurements.

**Table S2.** Ranges of parameters for scaling the normalized sum thermograms of RTC stages

| SOA System | Fresh Condition | RTC Condition | $\frac{\mathrm{VFR_{avg,RTC}}}{\mathrm{VFR_{avg,fresh}}}$ | $\alpha_{\mathrm{Mw}}$ | $\beta_{\rho_{\mathrm{org}}}$ |
|---|---|---|---|---|---|
| Low-$NO_x$ | Low RH, fresh | Low RH, RTC | [0.85, 0.91] | [0.98, 1.02] | [1, 1] |
| | High RH, fresh | High RH, RTC | [0.57, 0.73] | [1.02, 1.04] | [1.01, 1.01] |
| High-$NO_x$ | Low RH, fresh | Low RH, RTC | [0.89, 0.93] | [0.99, 1] | [1, 1] |
| | High RH, fresh | High RH, RTC | [0.67, 0.82] | [0.97, 1.09] | [0.99, 0.99] |

**Table S3.** Ranges of parameters for calculating the net change ratio (NCR) for each PMF sample factor

| SOA System | Ref. Condition | Condition j | $\frac{\mathrm{VFR_{avg,j}}}{\mathrm{VFR_{avg,ref}}}$ | $\alpha_{\mathrm{Mw}}$ | $\beta_{\rho_{\mathrm{org}}}$ |
|---|---|---|---|---|---|
| Low-$NO_x$ | Low RH, fresh | Low RH, RTC | [0.85, 0.91] | [0.98, 1.02] | [1, 1] |
| | | High RH, fresh | [0.77, 1.05] | [1.01, 1.10] | [0.99, 0.99] |
| | | High RH, RTC | [0.56, 0.60] | [1.03, 1.13] | [1, 1] |
| High-$NO_x$ | Low RH, fresh | Low RH, RTC | [0.89, 0.93] | [0.99, 1] | [1, 1] |
| | | High RH, fresh | [0.74, 0.95] | [0.97, 0.99] | [0.99, 0.99] |
| | | High RH, RTC | [0.61, 0.64] | [0.96, 1.06] | [0.98, 0.99] |

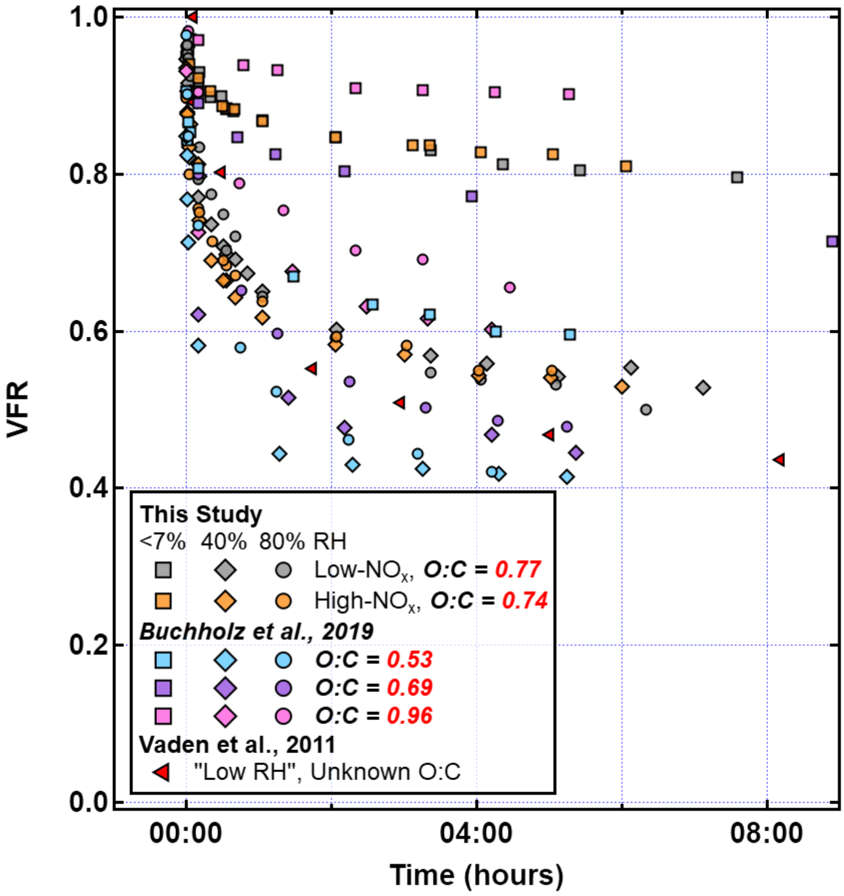

**Figure S1**. Comparison of evaporation behavior of α-pinene SOA particles in different studies, shown as VFR as function of evaporation time.

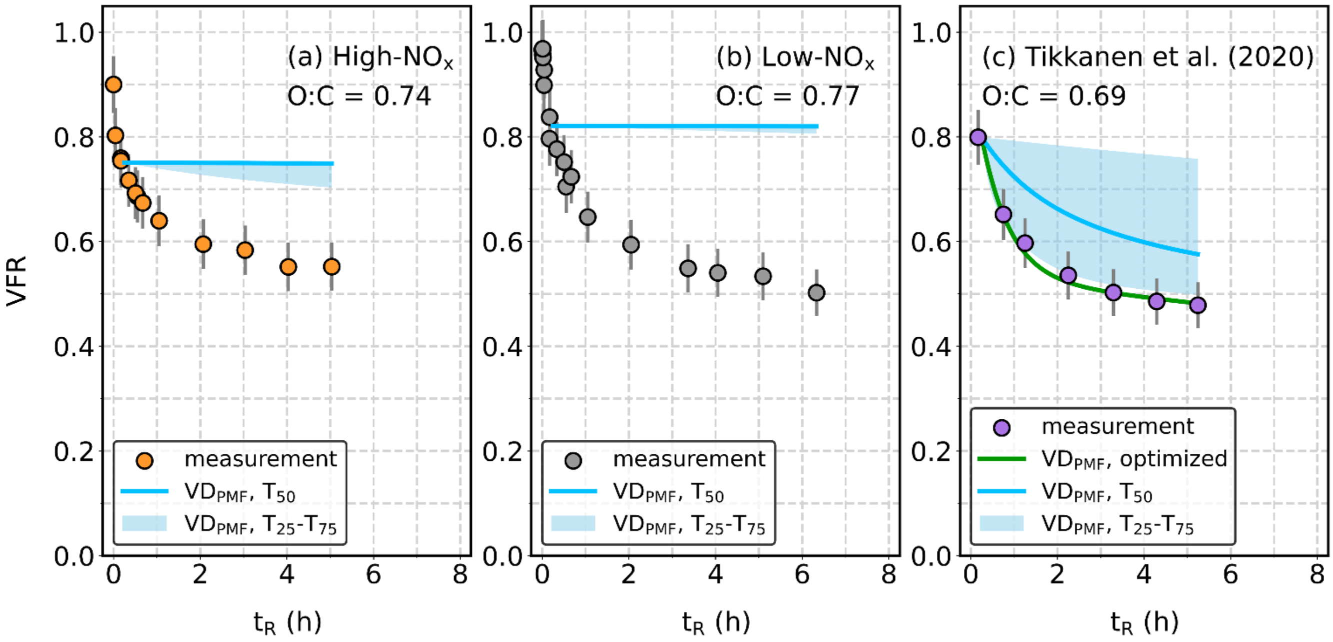

**Figure S2**. Measured (circles) and LLEVAP-simulated (lines) volume fraction reaming (VFR) as function of residence time ($t_R$) in the RTC for particles which evaporated under high RH (80% RH) conditions. The panels (a) and (b) show the results of α-pinene SOA particles which were formed under low-NO$_x$ (grey) and high-NO$_x$ (orange) conditions in the OFR, while panel (c) display the result of α-pinene SOA particles (O : C = 0.69) in Tikkanen et al. (2020). In each panel, the simulations were computed with the $T_{50}$ values (solid blue line) and $T_{25}$ – $T_{75}$ ranges (shaded areas in blue) of the volatility distributions obtained from the FIGAERO-CIMS data (VD$_{PMF}$). The simulation from the optimized VD$_{PMF}$ that was reported by Tikkanen et al. (2020) is shown in solid green line in the panel (c).

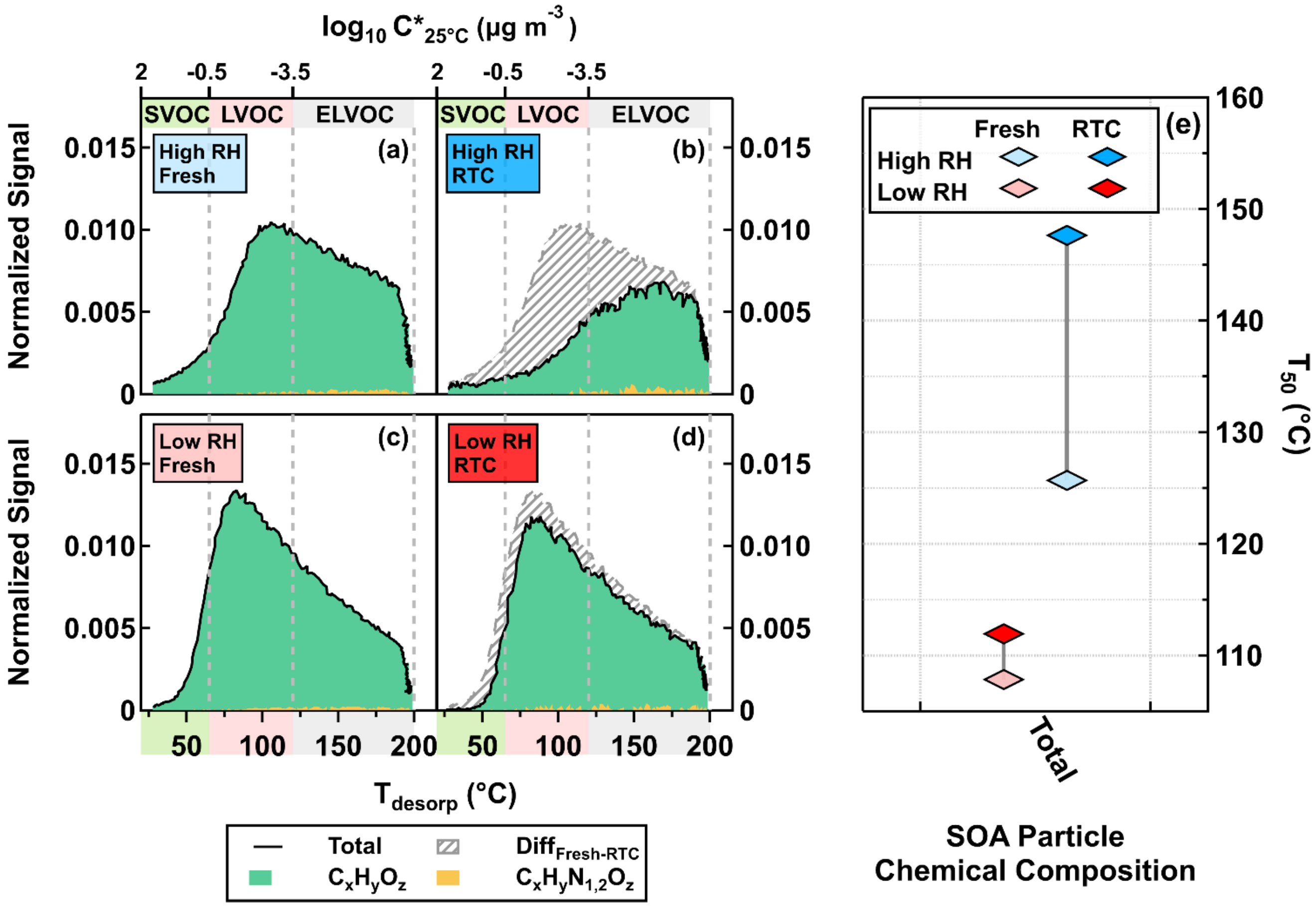

**Figure S3**. Sum thermograms (STG) (a – d) and median desorption temperature ($T_{50}$, diamonds) (e) for the low-$NO_x$ case under low RH (RH < 7 %) and high RH (80 % RH) conditions. CHO compounds and ON are indicated by $C_xH_yO_z$ and $C_xH_yN_{1,2}O_z$, respectively. On the panels (a – d), the solid black lines indicate the total signals of STGs with the green and yellow areas marking the contributions of $C_xH_yO_z$ and $C_xH_yN_{1,2}O_z$ to the STGs, respectively. The gray-striped areas represent the differences in STGs between fresh and RTC stages. The color bands on the abscissa indicate volatility classes. Note that we presented the STGs of RTC stages after accounting for changes in the average VFR ($VFR_{avg}$) between fresh and RTC stages during the FIGAERO sample time. As the signals of the ON were too low to derive reliable $T_{50}$ values, we only show the values for the total signal in panel (e).

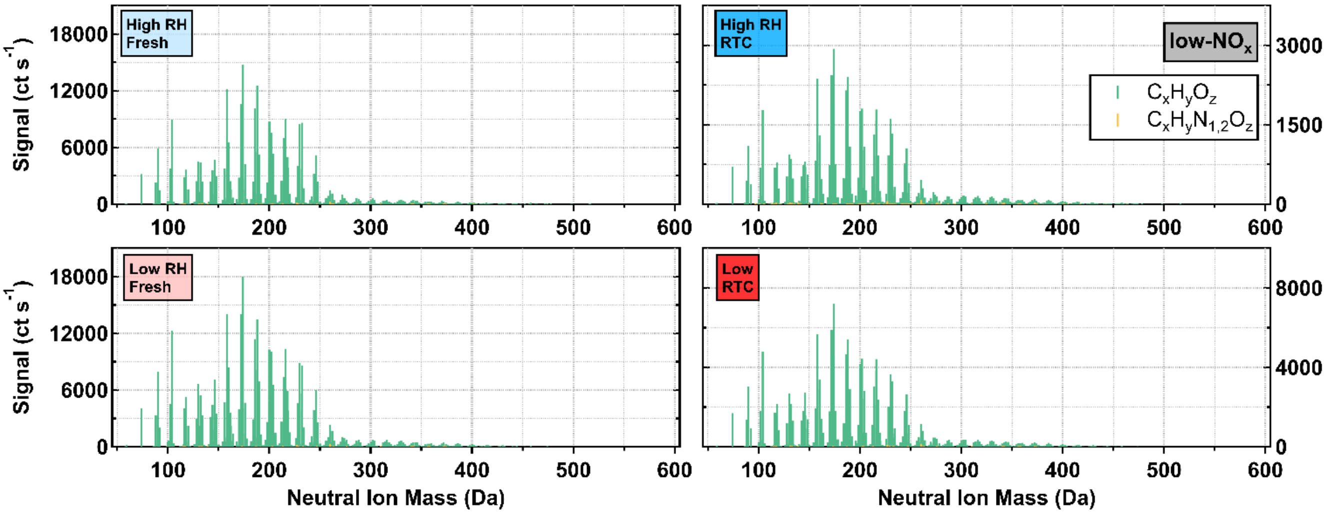

**Figure S4**. Integrated mass spectra for α-pinene SOA particles formed under low-NO$_x$ conditions in the OFR. CHO compounds and ON are colored with green and yellow, respectively.

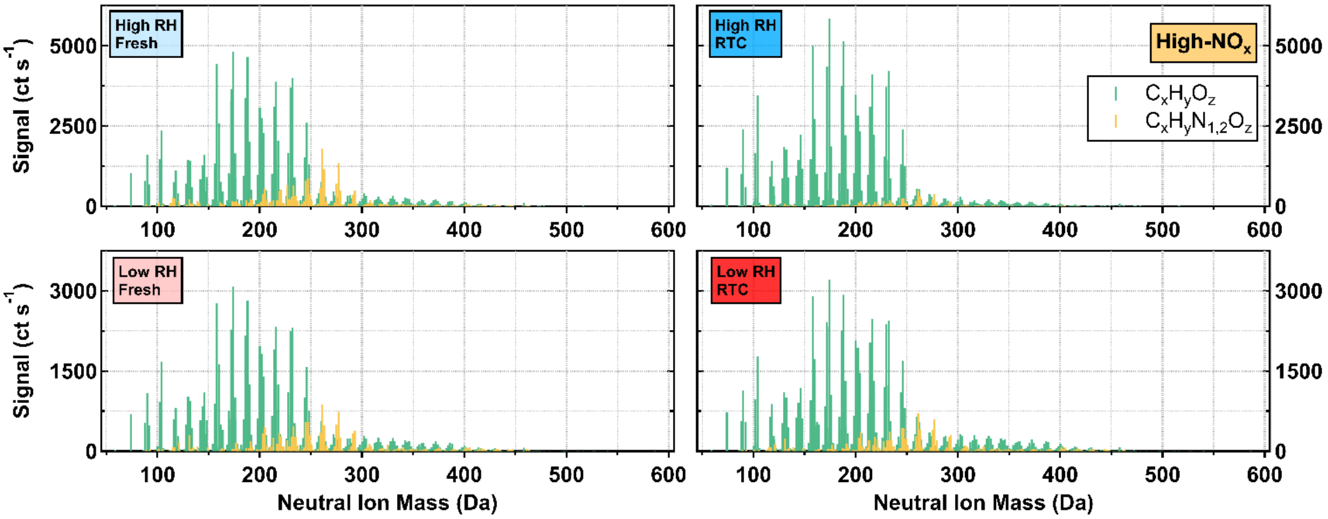

**Figure S5**. Integrated mass spectra for α-pinene SOA particles formed under high-NO$_x$ conditions in the OFR. CHO compounds and ON are colored with green and yellow, respectively.

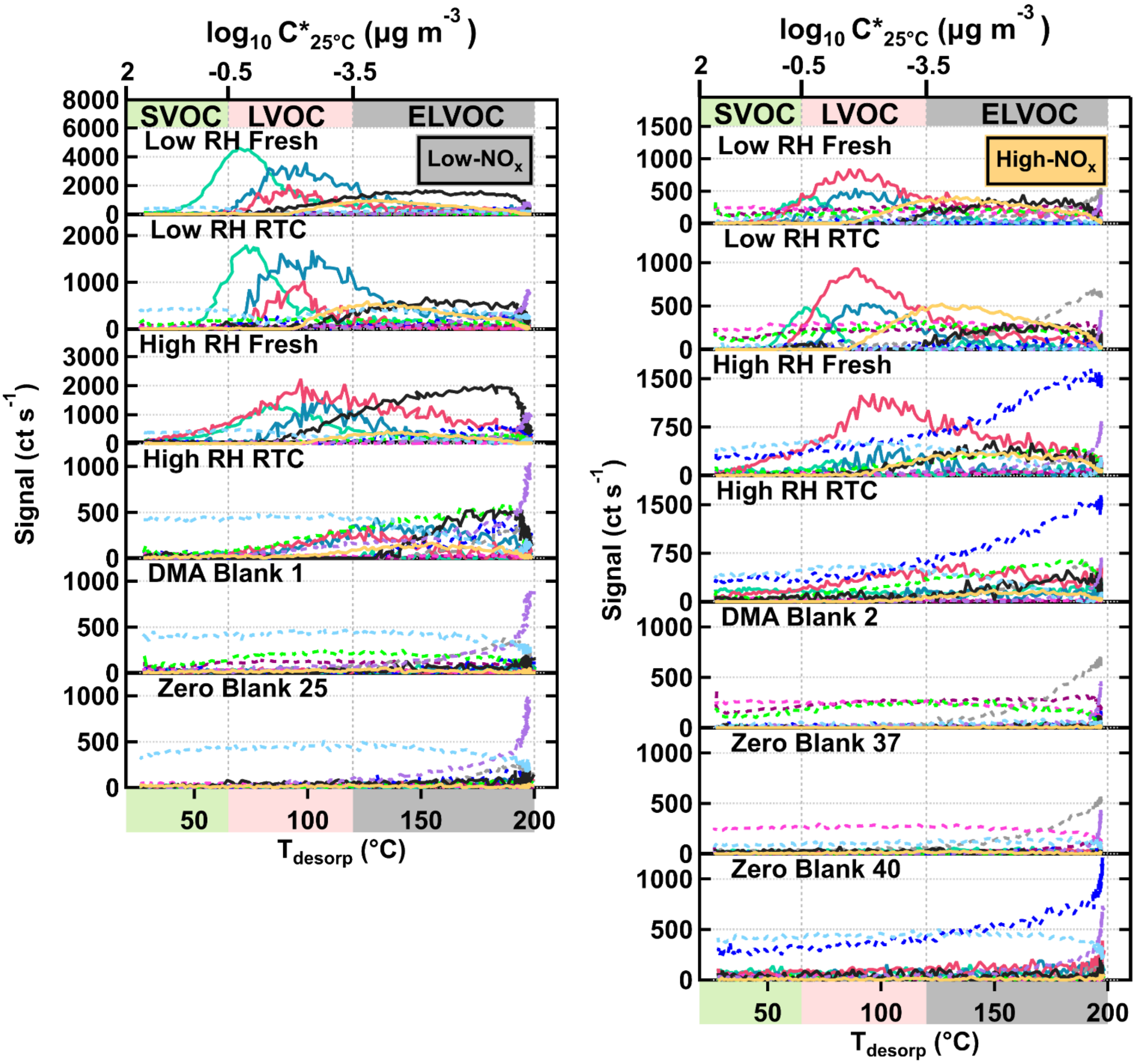

**Figure S6**. Sample (solid lines) and back (dashed lines) factors from a 12-factor solution of CHO compounds in α-pinene SOA particles which were formed under low-$NO_x$ and high-$NO_x$ conditions in the OFR. DMA blanks were determined by analyzing samples that were collected through the NanoDMAs with a set voltage of 0 V (i.e., no selected particles) for 0.5 hours. Zero blanks were investigated by measuring FIGAERO filters with no particle collection. In both columns, the desorption temperature ranges of different volatility classes are shown with color bands on the abscissa.

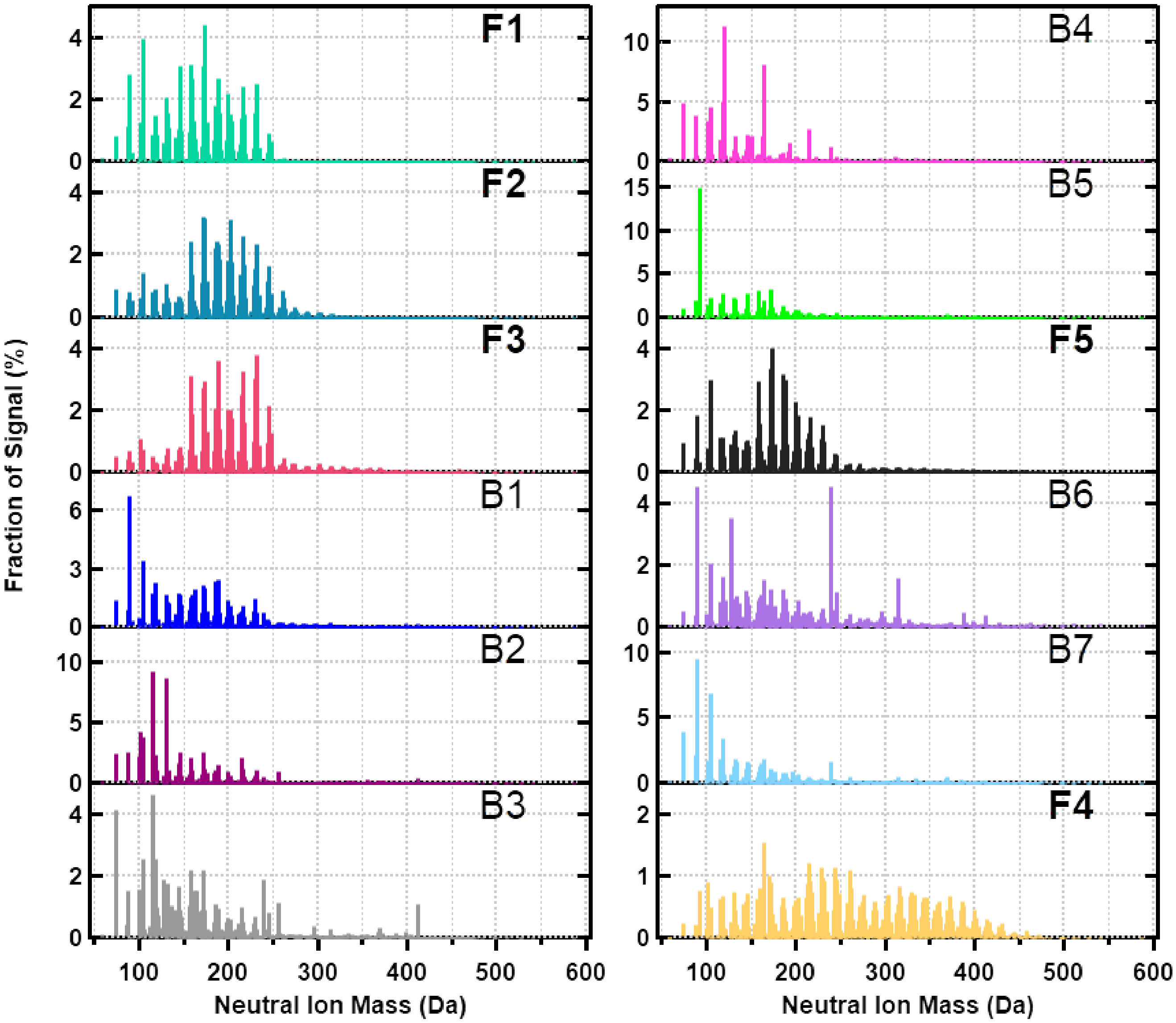

**Figure S7**. Normalized factor mass spectrums from a 12-factor solution of non-nitrated organics in α-pinene SOA particles.

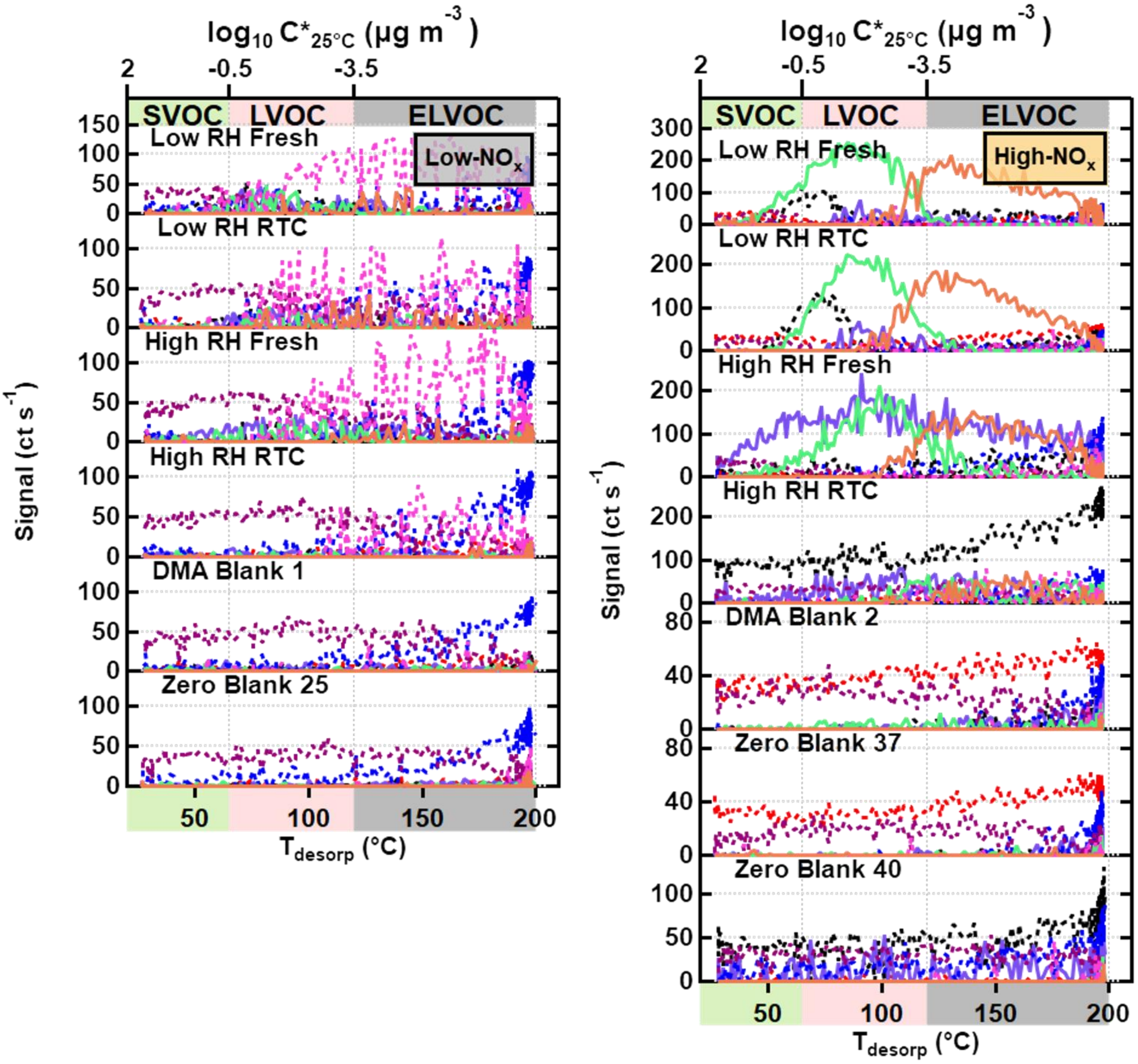

**Figure S8**. Sample (solid lines) and back (dashed lines) factors from an eight-factor solution of ON in α-pinene SOA particles that were formed under low-NO$_x$ and high-NO$_x$ conditions in the OFR. DMA blanks were determined by analyzing samples that were collected through the NanoDMAs with a set voltage of 0 V (i.e., no selected particles) for 0.5 hours. Zero blanks were investigated by measuring FIGAERO filters with no particle collection. In both columns, the ranges of desorption temperatures of different volatility classes are shown with color bands on the abscissa.

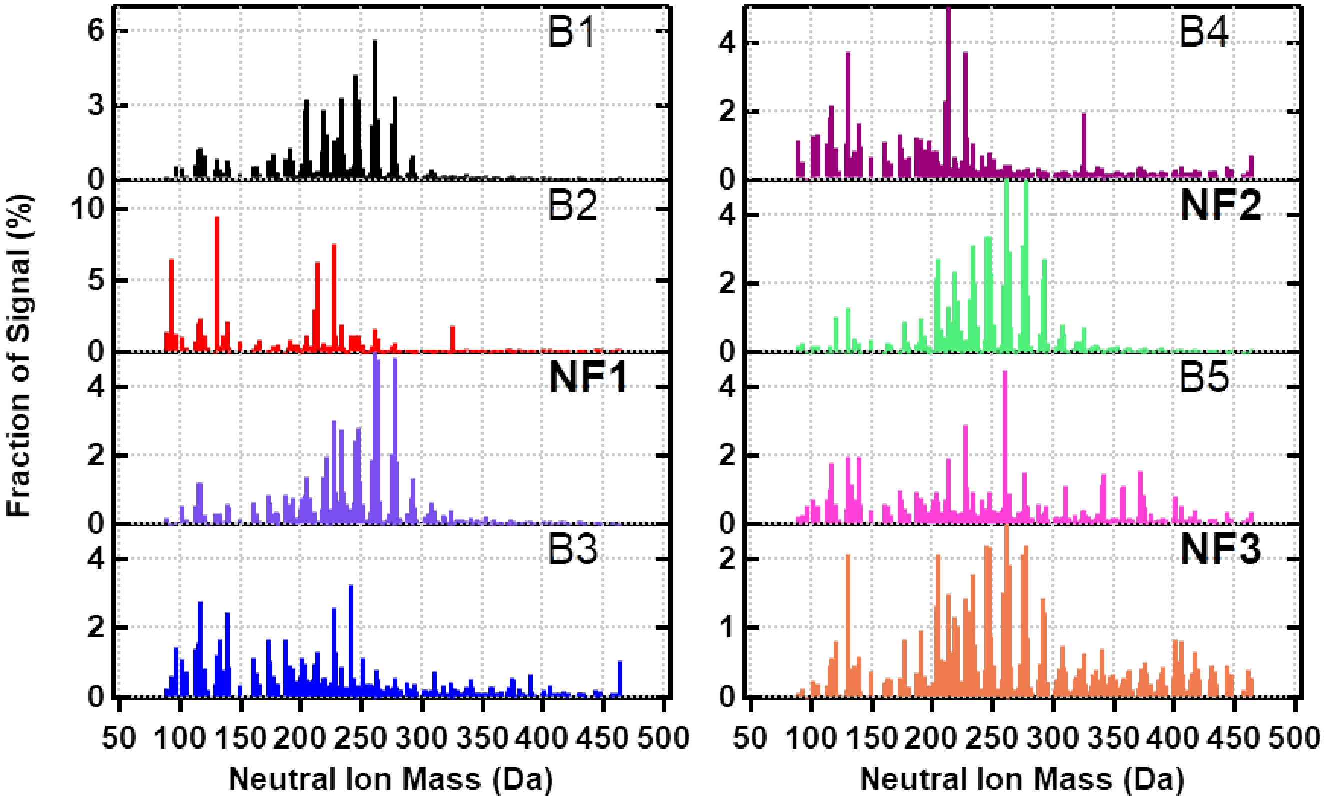

**Figure S9**. Normalized factor mass spectrums from an eight-factor solution of ON in α-pinene SOA particles.

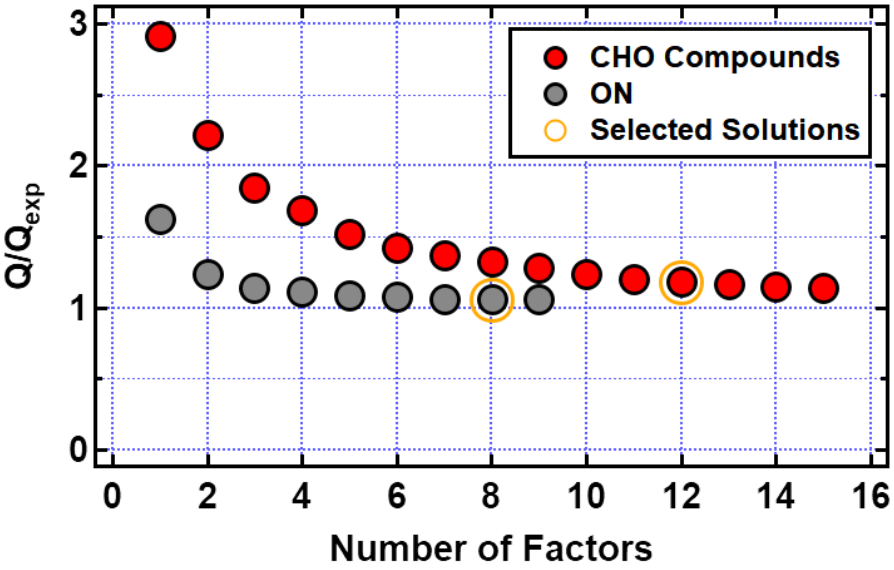

**Figure S10**. Q/$Q_{exp}$ values for PMF solutions for CHO compounds (red) and ON (gray) in α-pinene SOA particle data sets. Solutions chosen in the analysis are highlighted with orange circles.

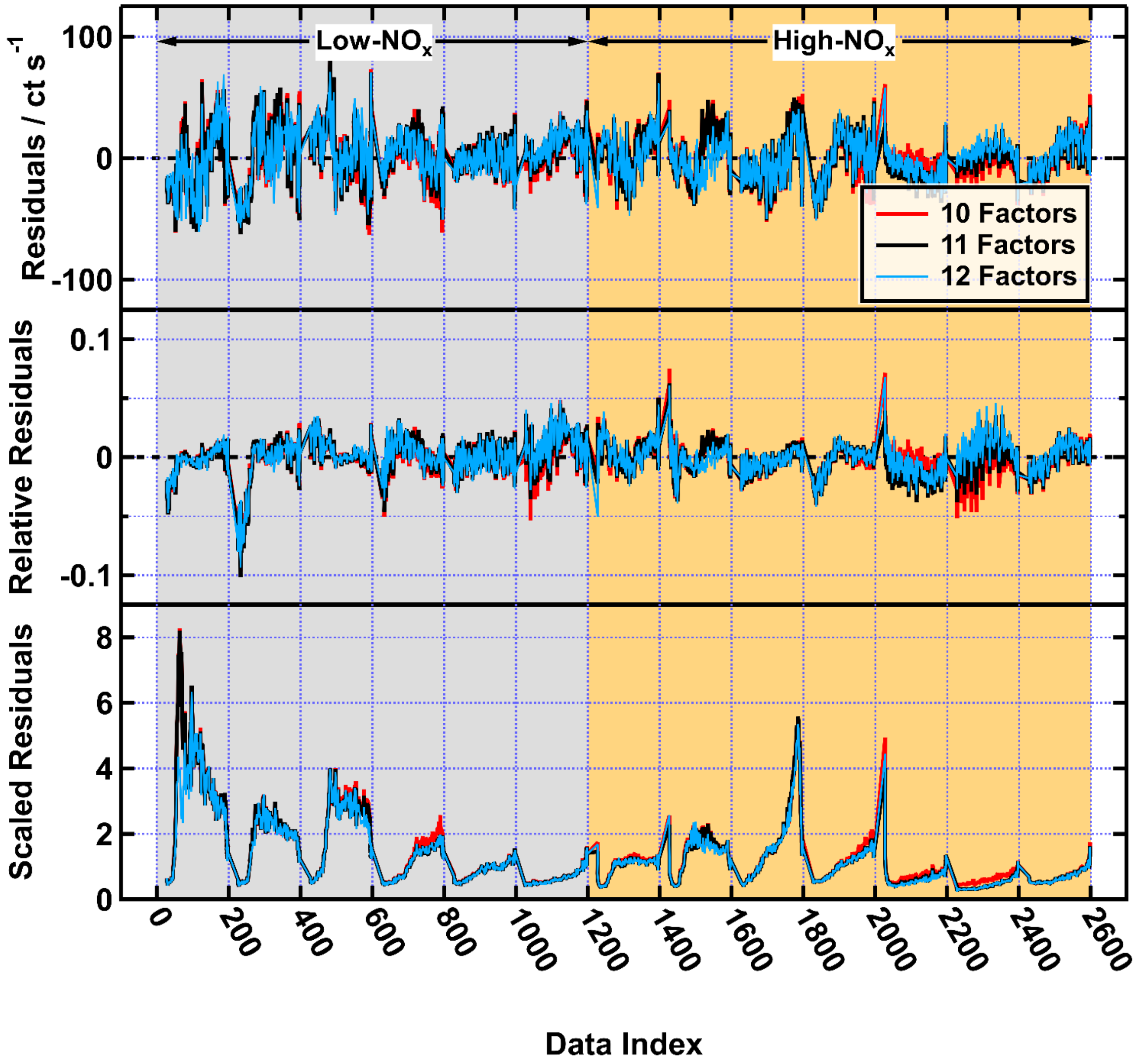

**Figure S11**. Residuals, relative residuals, and scaled residuals for the 10 – 12 factor solutions for the CHO compounds in α-pinene SOA particles. In the panel for the low-NO$_x$ condition (gray background), the order is: low RH, fresh (0 – 200); low RH, RTC (200 – 400); high RH, fresh (400 – 600); high RH, RTC (600 – 800); DMA blank 1 (800 – 1000); zero blank 25 (1000 – 1200). In the panel for the high-NO$_x$ condition (yellow background), the order is: low RH, fresh (1200 – 1400); low RH, RTC (1400 – 1600); high RH, fresh (1600 – 1800); high RH, RTC (1800 – 2000); DMA blank 2 (2000 – 2200); zero blank 37 (2200 – 2400); zero blank 40 (2400 – 2600).

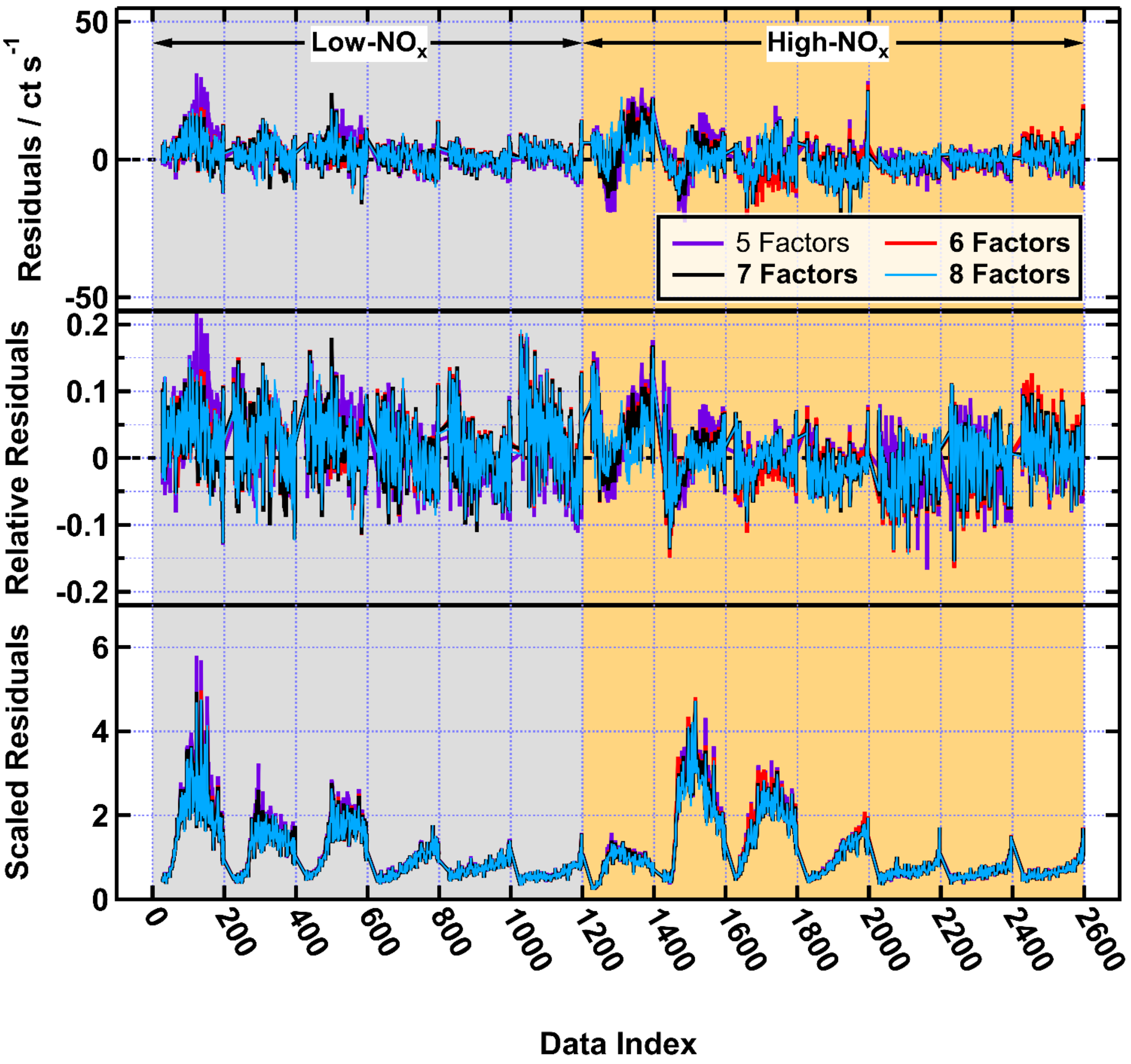

**Figure S12**. Residuals, relative residuals, and scaled residuals for the five – eight factor solutions for the ON in α-pinene SOA particles. In the panel for the low-NO$_x$ condition (gray background), the order is: low RH, fresh (0 – 200); low RH, RTC (200 – 400); high RH, fresh (400 – 600); high RH, RTC (600 – 800); DMA blank 1 (800 – 1000); zero blank 25 (1000 – 1200). In the panel for the high-NO$_x$ condition (yellow background), the order is: low RH, fresh (1200 – 1400); low RH, RTC (1400 – 1600); high RH, fresh (1600 – 1800); high RH, RTC (1800 – 2000); DMA blank 2 (2000 – 2200); zero blank 37 (2200 – 2400); zero blank 40 (2400 – 2600).

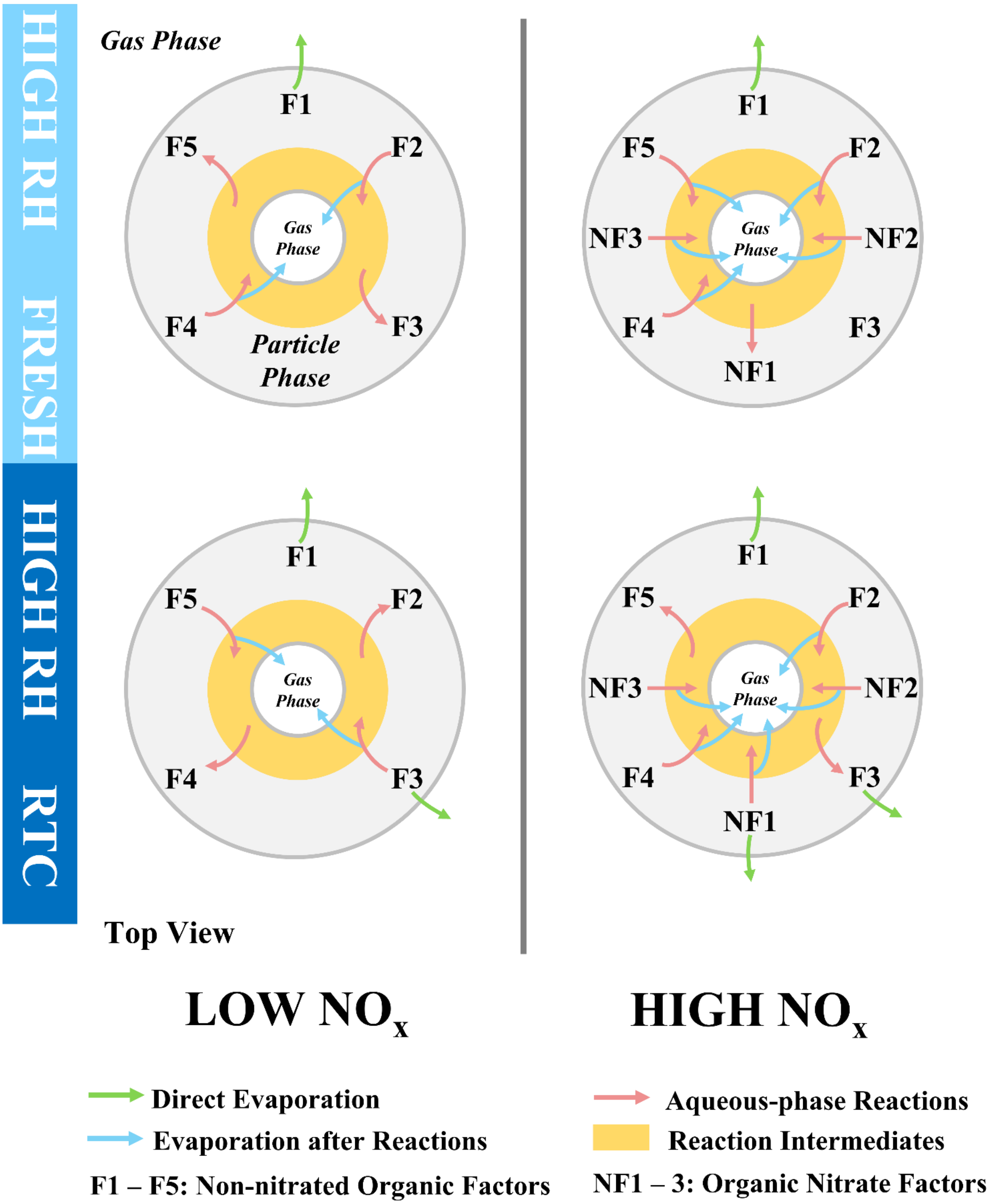

**Figure S13**. Processes during the isothermal evaporation of α-pinene SOA particles at two evaporation stage (fresh vs RTC) at high RH. Low-and high-NO$_x$ conditions indicate the levels of NO$_x$ during SOA formation in the OFR. Green and blue arrows suggest the loss pathways into gas phase due to direct evaporation and those due to evaporation after reactions, respectively. The yellow circles indicate the reaction intermediates formed in the aqueous-phase reactions that were shown in pink arrows. Pink arrows going into and out of the area of reactions intermediates represent aqueous-reactions consuming compounds of factors and those producing compounds of factors, respectively.